Lasers in Surgery and Medicine 21:464–473 (1997)

Imaging Temperature Changes in an Interventional 0.5 T Magnet: In-Vitro Results

Paul Steiner,[1] Andreas W. Schoenenberger,[1] Peter Erhart,[1] Erik Penner,[2] Gustav K. von Schulthess,[1] and Jörg F. Debatin[1]*

[1]MR-Center, Department of Radiology, University Hospital Zurich, CH-8091, Switzerland
[2]General Electric Medical Systems, Frankfurt, FRG

Background and Objective: **To evaluate the ability of monitoring laser induced temperature changes in an open, interventional 0.5T magnet, adopting fast T1-weighted sequences.**
Materials and Methods: **A fast gradient echo- (FGRE) and a fast spoiled gradient echo-sequence (FSPGR), both enabling an image update every 2.5 s, were investigated for their ability to visualize laser tissue effects at 5 Watt. Laser induced temperature was fluorooptically measured and correlated with signal intensity (SI) changes depicted by magnetic resonance imaging (MRI). MRI-lesions were compared with macroscopic findings.**
Results: **SI changes on FGRE images appeared as early as 15s following the onset of laser application and were significantly more pronounced than those seen on FSPGR images ($p < .0001$). A correlation of r = 0.94 (FGRE) and r = 0.92 (FSPGR) between temperature and SI loss was established. Owing to a steeper slope, the FGRE sequence was considered more sensitive to temperature changes. The areas of macroscopic tissue change correlated with those of SI loss, but lesion size was generally underestimated by MRI.**
Conclusion: **Laser monitoring is possible with rapid image updates in a midfield (0.5T) interventional MRI environment using fast gradient echo sequence designs. Lasers Surg. Med. 21:464–473, 1997.** **© 1997 Wiley-Liss, Inc.**

Key words: MRI; laser monitoring; longitudinal relaxation time; temperature imaging

INTRODUCTION

First described by Bown [1], interstitial laser photocoagulation (ILP) destroys tissues with near infrared, continuous wave laser energy, which is directed into a tissue volume through one or more interstitially implanted optical fibers. So far, ILP has been used to treat unresectable, localized human tumors in the brain [2], head and neck [3,4], as well as liver and breast [5,6]. The central problem of interstitial heating lies in the inability to predict size and geometry of the thermal lesions due to inherent tissue heterogeneities furthered by the variability of blood flow and tissue perfusion. Effective and reliable ILP does mandate however a means to assure laser coverage of the entire lesions without damage to healthy surrounding tissues. This requires on-line monitoring of laser-induced energy distribution while the application is ongoing. Ultrasound has shown some promise in this regard. Experiments in the liver and pancreas found it to be sensitive to acute tissue modifications induced by boiling tissue wa-

Contract grant sponsor: Deutsche Forschungsgemeinschaft; Contract grant number: STE 509/2–1; Contract grant sponsor: Cancer Committee of Zurich.

*Correspondence to: Jörg F. Debatin, M.D., Institute of Diagnostic Radiology, University Hospital Zurich, Rämistr 100, CH-8091 Zurich.

Accepted 7 May 1997

ter and diffusion of microbubbles in tissue structure [7,8]. Mere tissue heating could not be visualized.

The use of magnetic resonance imaging (MRI) in the diagnosis of different diseases has steadily increased over the past decade. In addition to its unsurpassed soft tissue contrast, the MRI experiment has been shown to be sensitive to changes in tissue temperature [9,10]. In fact there are three tissue properties, measurable with MRI that cause a reduction on signal intensity when tissue temperature increases: proton diffusivity [11], proton resonance frequency shifts [12] and the longitudinal nuclear spin relaxation time, T1 [13,14]. To date, most attempts to correlate MRI signal changes with heat-induced tissue damage during ILP have exploited the high signal-to-noise ratio inherent to high field (1.5 T and more) magnets [15,16]. In these magnet systems, patient access has remained limited. Simultaneous instrument manipulation and MRI-imaging is not possible.

Direct patient access is provided by a new midfield (0.5 T), superconductive, open-configurated MRI-system (Signa SP, GE Medical Systems, Milwaukee, WI). This MRI-system enables the integration of diagnostic imaging, tumor localization and monitoring of tumor laser-therapy. The latter is predicated upon a thorough assessment of the temperature sensitivity at 0.5 T.

This in-vitro study was performed to evaluate the ability to map the spatial and temporal distribution of laser effects on tissues in this open midfield system. The temperature correlation and sensitivity of two fast T1-weighted GRE sequences were assessed. In addition, lesion size as demonstrated on MR images was correlated with macroscopic findings.

MATERIALS AND METHODS

All experiments were performed on a 0.5-Tesla superconducting, open configurated MRI scanner (Signa SP, GE Medical Systems, Milwaukee, WI). Flexible surface coils were used for both RF-transmission and reception. An interactive workstation (Sun 4/670; Sun Microsystems, Mountain View, Calif.) was used for display and control of the continuously updated images.

A neodymium: yttrium aluminium garnet (Nd: YAG) laser (Versa Pulse Select, Coherent, Palo Alto, Calif.), emitting continuous output at a wavelength of 1064 nm, was used for all experiments. Positioned outside the scanner room to avoid safety hazards and corruption of the MRI-signal, the dual wave-length unit can be triggered by the interventionalist positioned next to the patient. A custom designed 10 m long laser cable bridges the distance between the Nd:YAG laser and a special connector installed within the wall of the scanner itself. The connector allows the fitting of fibres with different diameters and light distributers. Due to the special design of the long laser cable and connector box (Coherent), the power loss between generator and applicator amounted to merely 10%. For this study we used plastic-clad fiberoptic laser fibres (Dornier, Germering, FRG), which were equipped with a 1.9 mm × 20 mm cap made out of quartz glass. This cap is known to produce a more cylindrical distribution of light as opposed to a point source (plane-cut fiber).

In-vitro experiments were performed on a wooden phantom filled with minced porcine liver, as well as with explanted pig liver. For optimal image quality the objects were positioned at the isocenter of the magnet. Two different T1-weighted sequences, both allowing continuous image updates ever 2.5 s were evaluated:

(i) a fast gradient echo-sequence (FGRE) and
(ii) a fast spoiled gradient echo-sequence (FSPGR).

To assure a valid comparison of the data, identical parameters were employed for both sequences: TR/TE 20/10 ms, 50° flip angle, bandwidth 16 kHz, 1 NEX, 10 mm section thickness, 256 × 128 matrix, and 18 × 18 cm FOV.

Temperature Sensitivity

To determine the relationship between standardized temperature measurements and signal intensities for the two evaluated sequences, a wooden phantom measuring 8 × 8 × 8 cm was constructed. The phantom was filled with minced porcine liver tissue. While retaining the signal characteristics of liver, the grinding assured a relative homogeneity of the material and thereby a homogeneous temperature distribution. In each of the four walls a single hole was drilled: in two walls, opposite to one another, the holes were drilled in the midline 4 cm above ground; in the other two walls, midline holes were drilled 3.5 cm above ground. Upon withdrawal of an introducer, which traversed both 4 cm holes, the laser fibre applicator (laser tip) was positioned in the middle of the phantom at a level 4 cm above ground. Tem-

peratures were measured using a fluoroptic 4 sensor array probe (Luxtron, Santa Clara, Calif.). The sensors of the probe are spaced in 5 mm intervals. Similar to the laser fibre the temperature probe was positioned through an introducer traversing both 3.5 cm holes on opposing walls, crossing the laser fibre at a right angle. In the measurement plane 5 mm below the laser applicator, the temperature sensors remained unchanged in position throughout the experiments at fixed distances from the laser tip (1.5 and 6.5 mm) (Fig. 1).

Prior to laser irradiation the liver tissue was warmed to room temperature (20–22°C). Laser application was terminated, when the maximum measured temperature exceeded 75°C. Images were updated every 2.5 s and saved every 15 s for data analysis. ROIs, 3 mm in diameter were placed at a position corresponding to that of each thermosensor. For each ROI the percent SI-loss was calculated using the following equation:

$$\frac{SI\ (nl) - SI\ (las) \times 100}{SI\ (nl)}$$

where SI (las) corresponds to the signal intensity within the ROI during laser irradiation, and SI (nl) to the signal intensity within the same ROI prior to laser irradiation.

MRI-experiments were performed separately for each of the two evaluated sequences.

MRI Sensitivity to Laser Changes

These experiments were performed on explanted pig liver. The laser fiberoptic system was introduced into the hepatic tissue via a coaxial, 14-G, fully MRI-compatible needle system (BIP, Munich, Germany) [17]. The temperature measurement plane was optimised by means of 3 mm 'real time' imaging to identify the section containing the laser tip. At this position, 10 mm sections were acquired continuously using the two sequences, with imaging parameters outlined above.

Experiments were conducted with the laser output held constant at 5 W for a duration of 5 min. Updated every 2.5 s, images were saved for analysis every 15 s. Hence, in each experiment 21 images were available for quantitative analysis. For each of the two MRI-sequences, experiments were performed in triplicate. The percent signal intensity loss was calculated.

MRI-Signal Change vs. True Lesion Size

Laser induced lesions of different sizes were generated at a power settings of 5 W with the following irradiation times: 30, 45, 60, 90, 120, 150, 180, 250, and 300 s. For each experiment the lesion size as seen on the MR images was registered at the time of laser termination as well as following a cooling period of 5 min for experiments exceeding 90 s of irradiation and 3 min for shorter irradiation times. For each of the two evaluated sequences, three sets of experiments were performed for all time settings. Hence, a total of 54 laser applications were entered into the analysis. In MR-images the size of the signal altered areas, both at maximal temperature and following the cooling period, was determined based on the two diameters measurable in the acquisition plane traversing the laser fibre. Lesion size was calculated as the product of long and short axis lengths. Following each experiment the liver was dissected along the path of the laser fibre analogous to the imaging-plane. In the macroscopic specimen lesion size was determined in a fashion identical to that used in the MR images. Lesion diameters were measured with callipers. Size determinations of charred tissue were registered separately.

Statistical Analysis

The relationship between signal and temperature changes was described for the two evaluated sequences by linear regression analysis. Comparative analysis of the two evaluated sequences, with regard to laser induced percent SI change was based upon the unpaired two tailed Student's t-test. A p-value of less than 0.05 was considered significant. Similarly, the differences between imaging and macroscopic lesion sizes were comparable by unpaired Student's t-test.

RESULTS

There was good correlation between temperature and percent SI loss within the evaluated temperature range from 22–75°C. Linear regression analysis revealed correlation coefficients of 0.94 and 0.92 for the FGRE and FSPGR sequence respectively (Fig. 2). The FGRE sequence was found to be more sensitive to temperature change as is reflected by the steeper slope of 1.4 vs. 1.0 found for the FSPGR sequence.

The sensitivity of FGRE- and FSPGR-imaging toward laser induced temperature

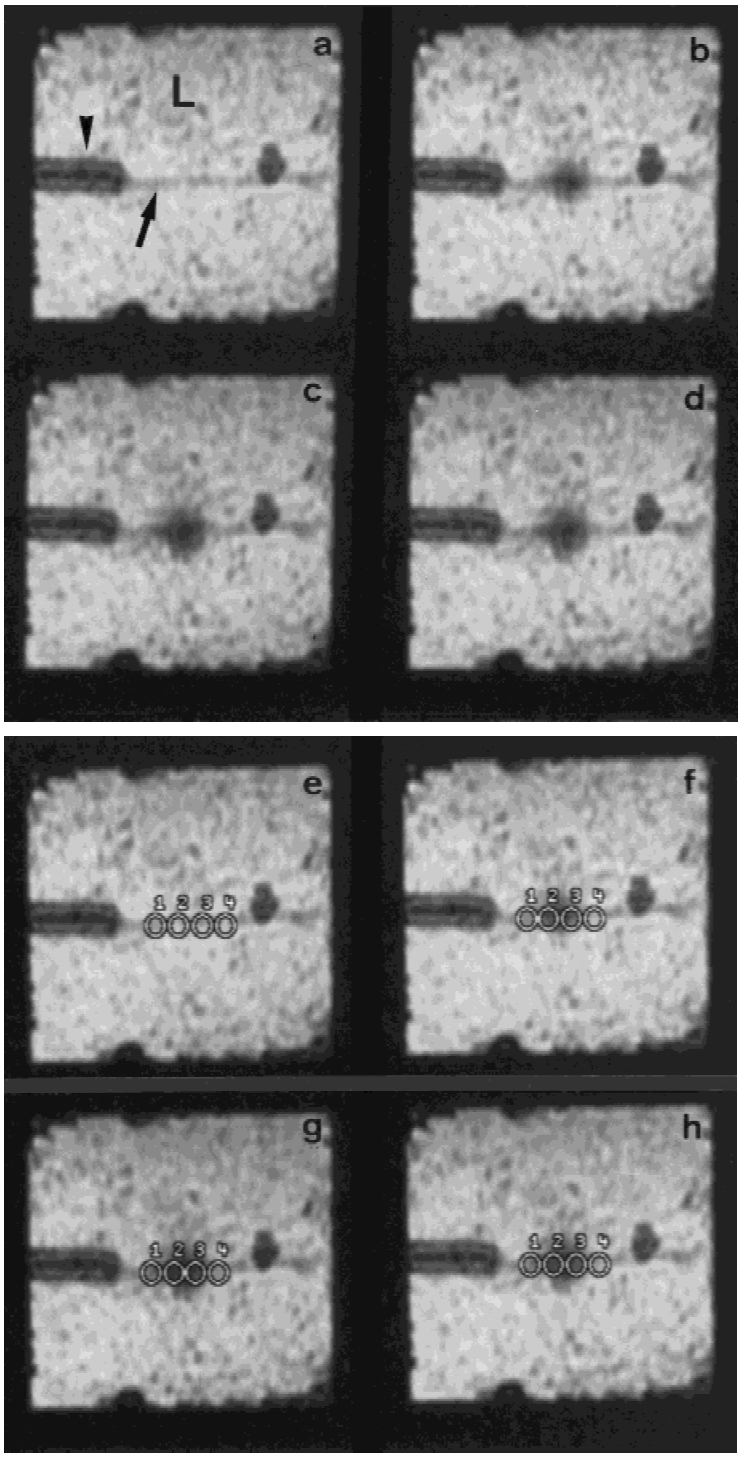

Fig. 1. Laser induced signal intensity (SI) change in correlation with local temperature, measured by four thermosensors. Images obtained from a FGRE experiment. **(a–d)** Phantom setup demonstrating the introducer (arrowhead) through which the temperature probe (solid arrow) was inserted into the minced porcine liver tissue (L). **(b–d)** demonstrate increasing size of SI change around the laser tip. The laser tip itself is located 5 mm below the MR-imaging plane and therefore not visible. **(e–h)** Circles representing 3 mm diameter region of interests for SI measurements. These were placed corresponding to the positions of the four thermosensors.

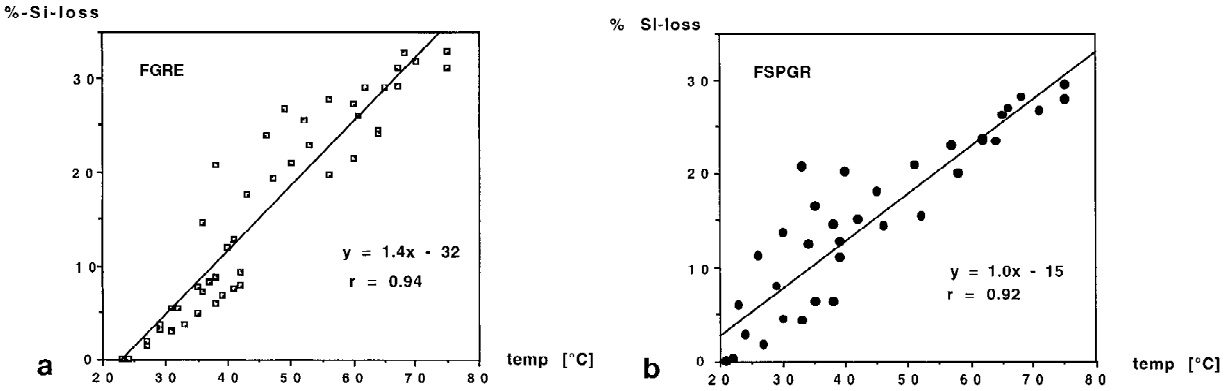

Fig. 2. Percent SI-loss (%-SI-loss) vs. temperature in minced porcine liver. Data were collected by FGRE **(a)** and FSPGR **(b)** over two separate measurements.

changes, measured as percent SI-loss over time is documented in Figure 3. Longer laser irradiation induced progressively greater signal changes. At all time settings greater signal changes were seen on the FGRE-images. On FGRE-images the average percent SI-loss ranged between 5 ± 0.1 % measured at 15 s and 33 ± 1.5 % determined at 300 s; on FSPGR images the changes were less pronounced ranging between 0.8 ± 0.2% and 27 ± 1.0%. The difference between relative SI-changes seen on FGRE and FSPGR images was statistically significant ($p < .0001$).

Lesions became macroscopically visible beyond a laser irradiation time of 60 s (Table 1). There was no FGRE MRI correlate in only one case at 60 s of irradiation. On FSPGR images there was no imaging correlate for laser irradiation times under 120 s. Four macroscopically visible lesions induced with 60 (n = 1) and 90 s (n = 3) of laser application were not seen on the FSPGR images. The smallest lesions visualized on FGRE and FSPGR images had a macroscopic size of 4 and 40 mm^2 respectively. Macroscopic lesion size was considerably underestimated on both image sets in 84% of cases on FGRE- and 87% on FSPGR-images. Figure 4 displays the correlation between maximal lesion size visualized on MRI and macroscopically documented tissue changes (FGRE: r = 0.98; FSPGR: r = 0.97).

Charred tissue became macroscopically visible beyond a laser irradiation time of 150 s (Fig. 5). The correlation between MRI lesion size following a period of cooling and macroscopical signs of charring was poorer for the FGRE sequence with a correlation coefficient of r = 0.79 compared to the FSPGR-images (r = 0.93). True, macroscopically verified size of charred tissue was underestimated to a far lesser extent than macroscopic coagulation lesion size. The comparison between FGRE and FSPGR concerning differences of macroscopical and MR-imaging measurements were of no statistical significance ($p = 0.7$ for maximal MRI-lesion size and $p = 0.1$ for minimal MRI-lesion size).

DISCUSSION

Temperature monitoring with MRI is possible at a field strength of 0.5 T (mid-field). Thus a first step towards effective and safe thermosensitive laser treatment delivery under MRI-guidance and monitoring appears to be fulfilled for this particular MRI system.

The 'open-configuration' scanner used in the presented experiments permits almost unhindered access to the patient. Percutaneously applied instruments can be manipulated by the interventionalist, while the region of interest within the patient is being imaged. MRI-tracking techniques [17] allow for continuous positional updates (20 updates/s) of the tip of any instrument in relation to a biplanar display of the surrounding tissues, including the presumed target lesion. Hence the position of a therapy delivery device can be altered on-line and monitored in real time, without changing the position of the patient. This allows for maximal positional and temporal flexibility regarding the delivery of laser treatment.

A generator providing safe and effective delivery of laser energy has been successfully installed into the MRI environment. Positioned outside the scanner room for safety and image quality reasons, but operated from within, this dual wave-length unit delivers laser energy to the applicator via a specially designed conduit assuring only minimal loss of laser energy.

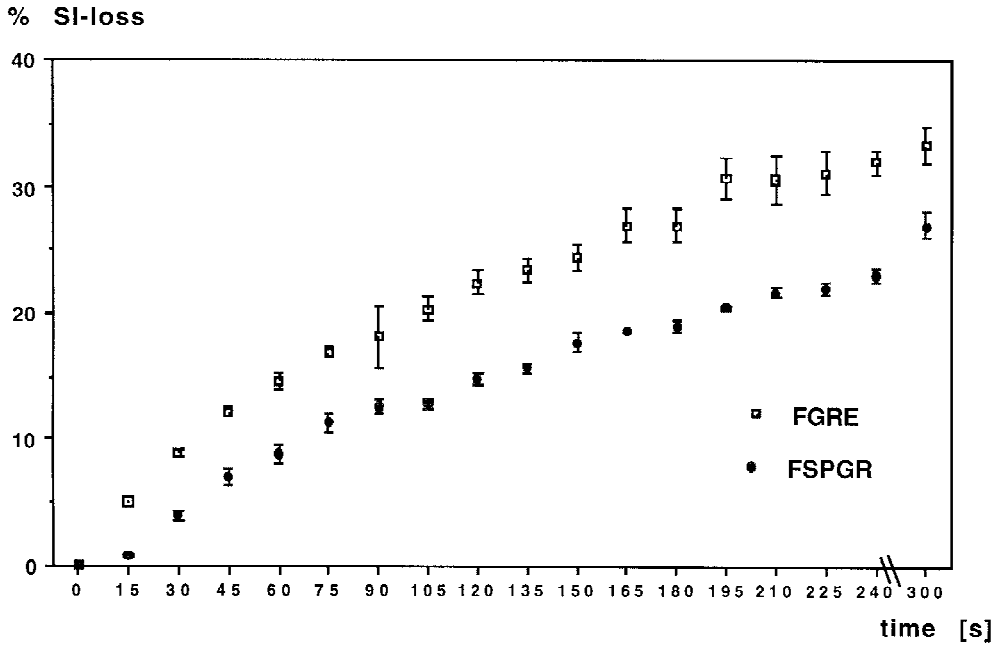

Fig. 3. Percent SI-loss (%-SI-loss) (±standard deviation) vs. time of laser irradiation for the FGRE- and FSPGR-sequences. Data are based on three separate measurements.

Finally, this study confirms the availability of temperature sensitive sequences, enabling the continuous monitoring of laser induced temperature changes by means of rapid image updates. In fact both evaluated fast gradient echo sequences may potentially be used to record temperature changes in an 0.5 T 'open' MRI environment.

A number of different MRI tissue properties are dependent on temperature. Thus, temperature maps have been successfully rendered using longitudinal nuclear spin relaxation times (T1) [16], proton diffusivity [11], proton resonance frequency shifts [12] or a combination of frequency shift and T1 changes [18]. While the various techniques are characterised by different advantages and disadvantages, all of these experimental studies were conducted on high-field MR-systems of at least 1.5 T field strength. The same holds true for the limited number of clinical studies available today [2,5,6,19]. The data presented in this study extends the basis of MRI temperature monitoring to include mid-field systems-a crucial extension in view of the limited patient access available with high field scanners.

In comparison to conventional spin-echo sequences, fast gradient-echo pulse sequences offer advantages in monitoring on-line ILP. The use of short TRs results in considerably shorter acquisition times without significant compromise in signal-to-noise. In fact, the use of fast gradient-echo sequence designs enables a temporal resolution of image updates in excess of thermal time constants inherent to most tissues [20]. To further enhance the T1-weighting of the sequence, spoiling gradients can be employed, virtually eliminating T2-effects. For the spoiled gradient echo-sequence a continuous phase shifting of the radiofrequency pulse is used to spoil residual transverse magnetization. The non-spoiled FGRE, especially when short TRs are used, builds up some T2* effect which contribute to image contrast. Nevertheless, it remains heavily T1-weighted.

This study revealed an almost linear correlation between laser induced temperature increase and SI-loss in liver tissue. The steeper slope of the curve fit found with FGRE is evidence of its greater sensitivity to temperature change. A finding which also has been reported by others at 1.5 T [21]. The increased temperature sensitivity of FGRE relative to FSPGR is also reflected by analysis of the laser induced tissue changes. Smaller lesions were detected almost 60 s earlier on FGRE-compared to FSPGR-images. A possible explanation might be that the T2* effect, in addition to the T1-weighting, synergistically contributes to the temperature induced SI change within FGRE images.

Both evaluated GRE sequences significantly underestimated the macroscopically confirmed lesion size. Beyond limited sensitivity to tempera-

TABLE 1. Correlation Between MRI-Data and Macroscopic Findings*

	FGRE				FSPGR			
time [s]	MRI-max [mm2]	macrosc. [mm2]	MRI-min. [mm2]	charring [mm2]	MRI-max [mm2]	macrosc. [mm2]	MRI-min. [mm2]	charring [mm2]
	140	224	30	12	160	240	15	15
300	209	247	18	21	198	247	8	12
	187	216	12	15	204	216	10	15
	117	180	24	8	98	98	12	8
240	135	160	15	12	130	180	10	8
	117	165	24	10	112	117	8	6
	96	140	9	12	45	80	4	4
180	96	108	8	6	96	140	6	4
	126	130	4	0	80	108	8	6
	56	60	9	0	70	77	0	0
150	80	45	4	0	56	60	0	0
	24	48	2	0	48	45	0	0
	42	60	2	0	42	50	0	0
120	40	55	0	0	40	60	0	0
	42	40	0	0	18	40	0	0
	20	25	0	0	0	30	0	0
90	15	24	0	0	0	16	0	0
	9	16	0	0	0	8	0	0
	0	0	0	0	0	4	0	0
60	0	2	0	0	0	0	0	0
	6	4	0	0	0	0	0	0
45	6	0	0	0	0	0	0	0
45 × 2	0	0	0	0	0	0	0	0
30 × 3	0	0	0	0	0	0	0	0

*Table summarizes FGRE and FSPGR data concerning the maximal area covered by in-vitro SI-changes at termination of laser irradiation (MRI-max). For irradiation, times ranged from 30–300 s, macroscopic lesion size (macrosc.), MRI lesion size following a cooling period (MRI-min) and macroscopically carbonized tissue (charring) were registered.

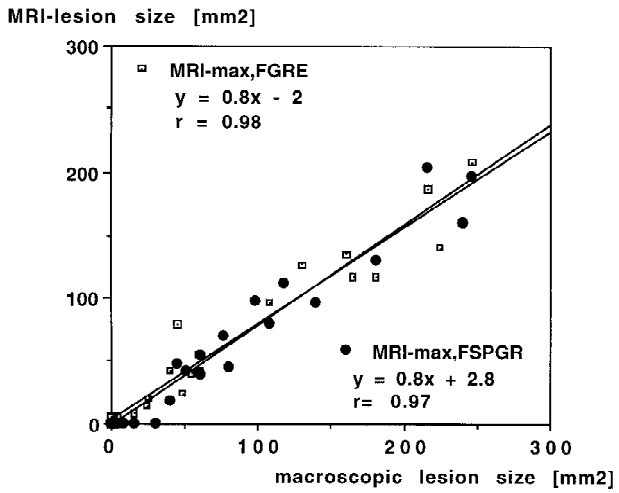

Fig. 4. Lesion size detected on MR imaging versus macroscopically verified lesion size. Data were obtained by FGRE- and FSPGR-sequences. The scatter diagram is based on the data from Table 1.

ture change of the evaluated sequences, there are several possible causes related to the experimental set-up in this particular study. The use of rather thick 10 mm sections introduced partial volume effects which artificially reduced the techniques sensitivity to temperature change. The use of a multiplanar sequence design, acquiring 3–5 thinner sections would mitigate this problem. Furthermore, the use of ex-vivo liver tissue increases the tissues disposition toward temperature induced charring and protein denaturation resulting in macroscopic tissue change. Under in-vivo conditions, tissue perfusion results in far steeper temperature gradients. Under those circumstances, a more accurate reflection of lesion size and SI change can be expected. Depending on the length of laser irradiation, under body temperature conditions of 37°C the visualization of a 20–30°C temperature change will be required.

Charred tissue or vaporized lesions with charred boarders could not be discriminated from surrounding coagulated tissue during laser energy deposition. Lesion size measured on images following a cooling period did reveal some correlation with charred tissues. The correlation with FSPGR images was better than with FGRE images. The differences were not pronounced however. It appears likely, that the use of contrast material will be better suited to enable the differ-

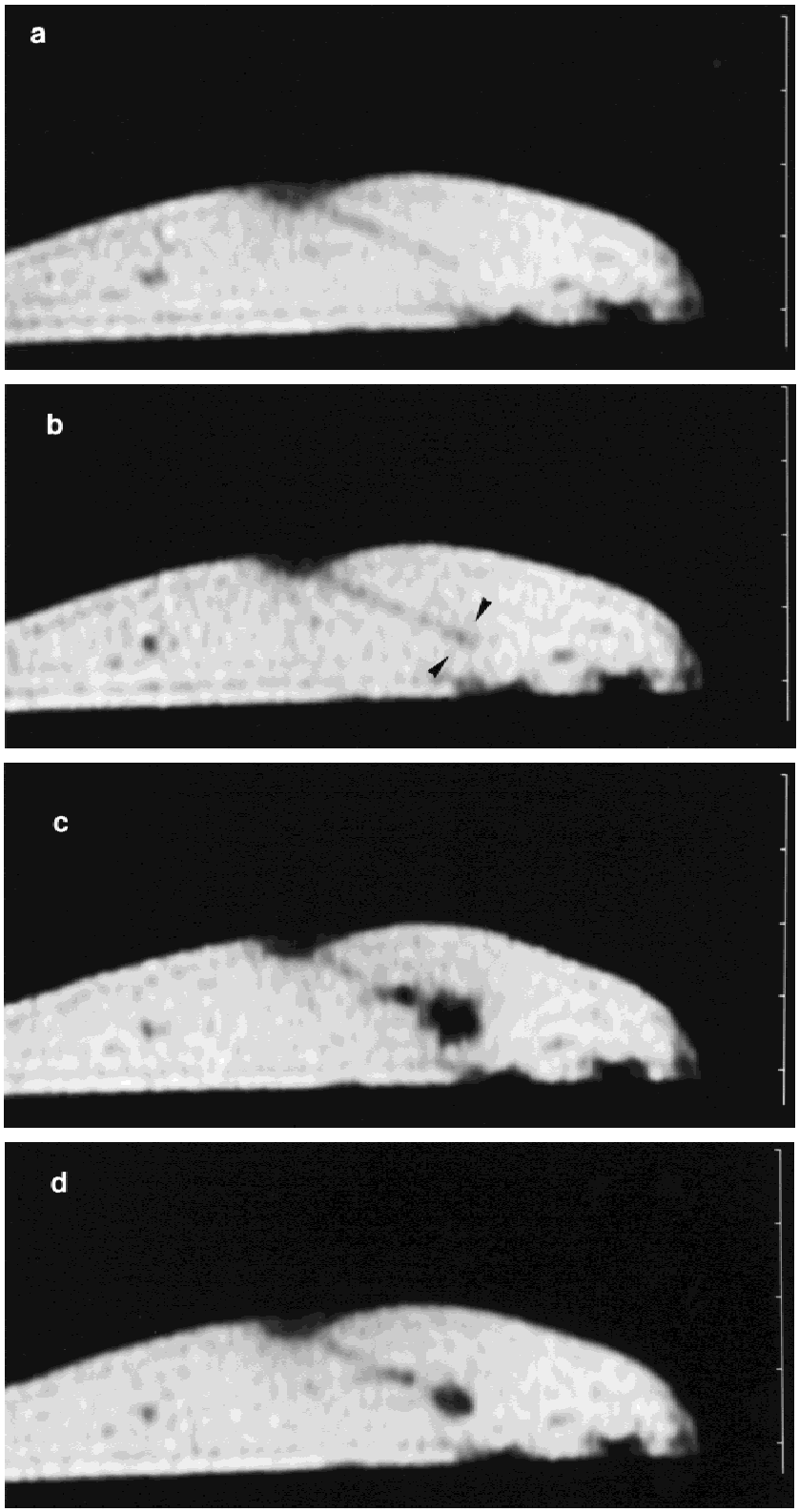

Fig. 5. **(a–d)** FGRE-images, monitoring a 5 W laser irradiation over 5 min in harvested porcine liver tissue. **(b)** SI decrease at the fibre tip was visualized as early as after 15 s of irradiation (arrowheads). **(c)** Lesion size visible immediately after 5 min of laser application and **(d)** following a cooling period of 5 min. The residual SI-loss in d) corresponded to vaporized tissue with charred boarders.

entiation of vital from immediately coagulated tissues.

Previous studies have pointed out the uncertainty in estimating absolute temperatures as a function of SI for liver tissue [16]. Within a temperature range of 30–70°C the 95% confidence interval was ±11°C [16]. The errors associated with temperature measurements derived from MR imaging limit its potential use in mapping thermal distributions in clinical applications. Several authors have therefore suggested that it would be sufficient to use MR imaging to detect laser induced tissue damage [13,22]. This approach would not offer much advantage over the use of sonography, which has indeed been shown to be insufficient to prevent damage to healthy tissues, whilst assuring destruction of the entire target lesion [23]. The reason for this observation lies in less than instantaneous cell death occurring after laser therapy. Mapping temperature change over time thus appears to be more promising. Commencing with a tissue-dependent baseline signal intensity, changes in temperature translate into relative SI changes. Since the magnitude of these relative changes is dependent on the baseline signal, some form of calibration for different tissues will be required. Subtraction of baseline from online images seems to provide a more reliable measure of therapeutic effectiveness or lack thereof.

Clearly, the in-vitro nature of the presented data limits its scope. In in-vivo studies in animals taking into account tissue perfusion and respiratory motion will be necessary to verify these findings. So far, we have only evaluated the two fastest T1-weighted sequences routinely available on the interventional 0.5 T scanner, both enabling almost real-time imaging. Optimization of temperature mapping might for example be achieved by adopting a technique which combines T1-weighted information as background image on which the temperature increase is superimposed according to proton resonance frequency shift changes [18]. A comparison between these alternative methods seems interesting, but was beyond the scope of this paper.

This study demonstrates that continuous update of temperature-sensitive images enables dynamic monitoring and thereby control of laser-tissue interaction in an interventional, open-configuration mid-field scanner. The evaluation and optimization of temperature related tissue changes in the 0.5 T environment must be considered a foundation for any future clinical application of thermosensitive therapies.

REFERENCES

1. Bown SG. Phototherapy of tumors. World J Surg 1983; 7:700–709.
2. Kahn T, Schwabe B, Bettag M, Harth T, Ulrich F, Rassek M, Schwarzmaier HJ, Mödder U. Mapping of the cortical motor hand area with functional MR imaging and MR imaging-guided laser-induced interstitial thermotherapy of brain tumors. Radiology 1996; 200:149–157.
3. Ohyama M, Nobori T, Moriyama I, Furuta S, Shima T. Laserthermia on head and neck malignancies: experimental and clinical studies. Acta Otolaryngol 1988; 458 Suppl:7–12.
4. Vogl TJ, Mack MG, Müller P, Philipp C, Juergens M, Knöbber D, Roggan A, Wust P, Jahnke V, Felix R. MR-guided laser-induced thermotherapy of tumors of the head and neck region: first clinical results. Fortschr Röntgenstr 1995; 163, 6:505–514.
5. Vogl TJ, Müller PK, Hammerstingl R, Weinhold N, Mack MG, Philipp C, Deimling M, Beuthan J, Pegios W, Riess H, Lemmens HP, Felix R. Malignant liver tumors treated with MR imaging-guided laser-induced thermotherapy: technique and prospective results. Radiology 1995; 196: 257–265.
6. Mumtaz H, Hall-Craggs MA, Wotherspoon A, Paley M, Buonaccorsi G, Amin Z, Wilkinson I, Kissin MW, Davidson TI, Taylor I, Bown SG. Laser therapy for breast cancer: MR imaging and histopathologic correlation. Radiology 1996; 200:651–658.
7. Steger AC, Lees WR, Walmsley K, Brown SG. Interstitial laser hyperthermia: a new approach to local destruction of tumors. Br Med J 1989; 299:362–365.
8. Dachman AH, McGehee JA, Beam TE, Burris JA, Powell DE. US-guided percutaneous laser ablation of liver tissue in a chronic pig model. Radiology 1990; 176:129–133.
9. Bottomly PA, Foster TH, Argersinger RE, Pfeifer LM. A review of normal tissue hydrogen NMR relaxation times and relaxation mechanisms from 1–100 Mhz: dependance on tissue type, NMR frequency, temperature, species, excision, and age. Med Phys 1984; 11:425–448.
10. Nelson TR, Tung SM. Temperature dependence of proton relaxation times in vitro. Magn Reson Imaging 1987; 5: 189–199.
11. Delannoy J, Chen CN, Turner R, Levin L, LeBihan D. Noninvasive temperature imaging using diffusion MRI. Magn Reson Med 1991; 19:333–339.
12. De Poorter J, De Wagter C, De Deene Y, Thomsen C, Stahlberg F, Achten E. Noninvasive MRI thermometry with the proton resonance frequency method: in vivo results in human muscle. Magn Reson Med 1995; 33:74–81.
13. Tracz RA, Wyman DR, Little PB, Towner RA, Stewart WA, Schatz SW, Wilson BC, Pennock PW, Janzen EG. Comparison of magnetic resonance images and histopathological findings of lesions induced by interstitial laser photocoagulation in the brain. Lasers Surg Med 1993; 13:45–54.
14. Matsumoto R, Oshio K, Jolesz FA. Monitoring of laser and freezing induced ablation in the liver with T1-weighted MR-imaging. J Magn Reson Imaging 1992; 2: 555–562.
15. Jolesz FA, Bleier AR, Jakab P, Ruenzel PW, Huttl K, Jako GJ. MR imaging of laser-tissue interactions. Radiology 1988; 168:249–253.
16. Pignoli E, Marchesini R, Curti L, Sichirollo AE, Tomatis

S, Musumeci R. Potential and limitations of magnetic resonance imaging for real-time monitoring of interstitial laser phototherapy. Acad Radiol 1995; 2:741–747.

17. Leung DA, Debatin JF, Wildermuth S, Heske N, Dumoulin CL, Darrow RD, Hauser M, Davis CP, von Schulthess GK. Real-time biplanar needle tracking for interventional MR imaging procedures. Radiology 1995; 197:485–488.
18. Cline HE, Hynynen K, Schneider E, Hardy CJ, Maier SE, Watkins RD, Jolesz FA. Simultaneous magnetic resonance phase and magnitude temperature maps in muscle. Magn Reson Med 1996; 35:309–315.
19. Vogl TJ, Weinhold N, Müller P, Phillip C, Roggan A, Mack MG, Balzer JO, Eichstädt H, Blumhardt G, Lobeck H, Felix R. Early clinical experience with pre-operative MR-guided laser-induced thermotherapy (LITT) of liver metastases. Fortschr Röntgenstr 1996; 164, 5:413–421.
20. Svaasand LO, Gomer CJ, Welch AJ. In: Muller GJ, Sliney DH, eds. Dosimetry of Laser Radiation in Medicine and Biology. SPIE Optical Engineering Press, Bellingham, WA., 1989.
21. Cline HE, Hynynen K, Hardy CJ, Watkins RD, Schenk JF, Jolesz FA. MR temperature mapping of focused ultrasound surgery. Magn Reson Med 1994; 31:628–636.
22. Tracz RA, Wyman DR, Little PB, Towner RA, Stewart WA, Schatz SW, Pennock PW, Wilson BC. Magnetic resonance imaging of interstitial laser photocoagulation in brain. Lasers Surg Med 1992; 12:165–173.
23. Godlewski G, Bourgeois JM, Sambuc P, Gouze C, Ould-Said H, Eledjam JJ. Rouy S, Pignodel C. Ultrasonic and histopathologic correlations of deep focal hepatic lesions induced by stereotaxic Nd-YAG laser applications. Ultrasound Med Biol 1988; 14:287–291.